Influence of iron dilution on plastic deformation mechanisms in cobalt-based alloys: Consequence of phase transformations on tribological behavior

Christine Boher, Tarek Younsi, Adriana Soveja, Michel Chaussumier

Influence of iron dilution on plastic deformation mechanisms in cobalt-based alloys: Consequence of phase transformations on tribological behavior

Christine Boher [a,*], Tarek Younsi [a], Adriana Soveja [b], Michel Chaussumier [c]

[a] Institut Clément-Ader (ICA), Université de Toulouse, CNRS, IMT Mines Albi, INSA, ISAE–SUPAERO, UPS, Campus Jarlard, 81013, Albi, France
[b] Institut Clément Ader (ICA), UMR CNRS 5312, Université de Toulouse, IMT Mines Albi, INSA, ISAE, UPS, 3 Rue Caroline Aigle, 31000, Toulouse, France
[c] Institut Clément Ader (ICA), UMR CNRS 5312, Université de Toulouse, IMT Mines Albi, INSA, ISAE, UPS, 135, Avenue de Rangueil, 31077, Toulouse Cedex 4, France

The chemical composition and microstructure of metallic parts are parameters that affect plastic deformation accommodation mechanisms under friction stresses. The content of alloying elements impacts the stacking fault energy and the plastic deformation, and thus affects the tribological behavior. Depending on this content and the levels of mechanical stresses, plastic deformation of some alloys obtained under non-equilibrium conditions can occur. It is caused by different mechanisms, such as perfect slip and/or partial dislocation slip, as well as by phase transformation. The purpose of this study is to determine the influence of the plastic deformation accommodation mechanisms on tribological behavior by studying the effect of the iron content in cobalt-based alloys. For manufacturing purposes, cobalt-based coatings are produced on steel substrate using a additive manufacturing process (SLM). With this process, the microstructures of the cobalt-based coatings are essentially metastable FCC phase at room temperature with different contents of diluted iron. Tribological tests were carried out with a ball-to-disc contact. Iron contents were estimated by EDS-SEM. Analytical techniques such as XRD and EBSD were used to identify the microstructural changes observed in TTS due to tribological loading. The friction coefficient is linked to the evolution of the plastic deformation mechanisms activated to accommodate the contact. In particular, in addition to work-hardening phenomena, phase transformations are possible, namely a metastable FCC phase gives an HCP phase and a metastable FCC phase gives an α′-BCC phase under tribological loading. Both types of transformations can occur, individually or simultaneously, depending on the iron content in the coating.

1. Introduction

Cobalt-based alloys are often used as thick coatings on steel substrate to improve surface properties, such as wear, oxidation, and corrosion resistance [1,2]. To produce CoCrMo coatings on a steel substrate sur-face, different depositing processes can be used, such as Metal Inert Gas MIG [3], laser cladding [4–6] or spraying processes [4]. Depending on the input energy densities involved in coating processes, iron dilution from substrate into coatings of the CoCrMo alloy can occur [3,4].

In addition, according to phase diagrams, cobalt crystallizes into a Face Cubic Centered (FCC) structure at a high temperature and into a Hexagonal Compact (HCP) structure at room temperature. The temperature of the allotropic transformation of FCC phase into HCP phase is 417 °C. Because of high cooling rates induced by quenching during the depositing processes mentioned above, the crystalline structure of the CoCrMo coating remains FCC at room temperature, but in a meta-equilibium state.

At ambient temperature, several plasticity mechanisms are involved in metallic parts subject to mechanical stresses. Work hardening, which is the result of an increase in the number of blocking points for dislocation gliding, counteracts the increase in the number of dislocations, which leads to tangles of dislocations [8] and modifies the reversibility threshold of the plastic deformation. Changes in the sequence of the crystal lattices mechanical twinning or mechanical allotropic phase transformation also allow some metallic materials to accommodate plastic deformation. These phase transformations are martensitic in

nature and occur without atomic diffusion. To describe martensitic transformation, Christian et al. gave the following definition: a martensitic transformation is a shear dominant, lattice distortive, diffusionless transformation occurring by nucleation and growth (of the transformation) [24].

These last mechanisms are found in metallic materials with a compact crystal structure (FCC or HCP), in which the presence of some atoms in solid solution significantly modifies the stacking-fault energy (SFE), such as austenitic TWIP steels (for TWinning Induced Plasticity), shape memory alloys (TiNi, CuZnAl, CuAlNi) or cobalt-based alloys. A low stacking-fault energy is associated with a large dissociation distance between the Shockley partial dislocations, which favors the dissociation of the perfect dislocation into two partial dislocations and thus facili-tates the phase transformation of, for instance, a metastable FCC phase into an HCP phase. A high stacking-fault energy, on the other hand, slows down the initiation of defects and thus the dissociation of dislo-cations, consequently delaying the phase transformation [7].

With regard to cobalt-based alloy coatings, chemical elements such as chromium, molybdenum and tungsten stabilize the HCP phase. They contribute to a weakening of the atomic bonds and an increase in the distortion distance in the stacking fault plane. The result is a decrease in the energy of the stacking faults (-84 mJ/m^2 $\leq$SFE ≤ -25 mJ/m^2) in cobalt-based alloys compared to pure cobalt (SFE $= 0.15$ mJ/m^2), which facilitates the dissociation of dislocations, confirming what was announced by Ref. [9], namely an SFE which becomes negative compared to that of pure cobalt. These elements consequently increase the phase transition temperature, which is in the order of 649–760 °C in cobalt-based alloys [1,7]. In contrast, elements such as iron, manganese and nickel stabilize the FCC phase by decreasing the charge density in the stacking fault regions. They tend to decrease the distortion distance and consequently increase the stacking fault energy, which slows down the formation of partial dislocations and thus delays the phase change of metastable FCC phase into HCP phase [1,7,9,10].

As regards cobalt-based alloy coatings obtained by fast cooling processes (MIG, laser cladding and spraying processes), these present a metastable FCC phase, while their microstructure is made of dendrites surrounded by hard carbides [3–5,11]. The iron content, due to dilution of the steel substrate, increases the stacking-fault energy. This fact has a direct influence on the plastic deformation mechanisms of Cobalt alloys [7] under mechanical solicitations such as tribological ones. They can be transformed into an HCP structure after mechanical solicitations that induce plastic strains. The FCC phase into HCP phase transformation is martensitic in nature and occurs without diffusion. It is known as plastic strain-induced phase transformation.

The authors investigate the tribological behavior of cobalt-based hardfacings under sliding wear [3]. They study a monolayer MIG hardfacing and a multilayer laser hardfacing, differing mainly in their iron content. Under tribological sollicitations, they show that the plasticity mechanisms involved can be perfect dislocation gliding and/or FCC into HCP phase transformation. These mechanisms particularly depend on the iron content, and so on the stacking-fault energy. A relationship is demonstrated between the friction coefficient evolution and the FCC into HCP phase transformation (i.e. the HCP content in the TTS).

The aim of this experimental work is to understand the role of plastic deformation mechanisms in tribological behaviour. To allow different plastic deformation mechanisms to be involved in the tribological con-tact, we decided to study the influence of the dilution content of iron in cobalt-based coatings on the tribological properties. The content of iron in the cobalt based coatings induces different crystallographic phases that influence the plasticity mechanisms of Tribologically Transformed Surfaces (TTS) under tribological solicitations, and thus the behavior of the frictional surfaces. The SLM process was only carried out to perform cobalt-based alloy coatings on steel substrate and to permit iron dilution.

2. Devices

2.1. SLM coating device

An additive manufacturing device was employed to achieve the cobalt-based coatings on steel substrate. This process, using powder bed technology, is known as the Selective Laser Melting process. It uses high power to melt and fuse metal powder layer by layer. It provides very high accuracy in manufactured parts because of the small size of the laser spot and the layer thickness, which is usually between 20 and 100 μm [12].

In this study, the SLM Solution (SLM125HL) was used with a 1070 nm wavelength Nd:YAG laser operating in continuous mode and delivering a maximum power of 400 W. The focused laser spot size is around 80 μm in diameter. The SLM parameters are given in Table 1 and are those recommended by the SLM Solution supplier. The hatching (or hatch distance) is the distance between two consecutive laser scan tracks. Some studies give the hatching as equal to the laser diameter [13] but others give the hatching as greater [15,16] or less [14] than the laser diameter, depending on the SLM manufacturing strategy. It is explained in the literature that when the laser spot is focused, the melt pool can influence 2–3 neighboring scanning tracks [13]. In this study, the scan direction rotates by 60° between two successive layers, so the laser track returns to the same direction every 3 layers (Fig. 1). No post-treatments (thermal treatment or grinding or polishing) were applied on the sam-ples after the SLM process.

2.2. Tribological device

The tribometer was a ball-on-disc type CSM Instruments tribometer with a rotating disc (Fig. 2). The tests were performed at room temperature. The normal load was applied by dead weights. During the friction test, the tangential sliding forces Ft were measured by the deflection of a spring arm and LVDT sensors. The cobalt-based alloyed coatings were applied to the entire surface of the disc with a diameter of $\Theta = 55$ mm.

The counterpart is a ball made of alumina Al_2O_3 with a radius of 3 mm. The choice of this grade is justified by the higher hardness of alumina compared to cobalt-based alloys and by the fact that alumina does not contain iron.

The same normal loading, rotationnal speed and number of laps were used for all the tribological tests (Table 2). For all new tribological test runs, the counterpart was always a new Al_2O_3 ball. One sample for a fixed number of layers is tested in this work. The friction curves, the average values and standard deviation of the friction coefficients were directly calculated by the Tribometer software (Instrument X).

A preliminary study showed that for a fixed number of layers (4-layers), changing the SLM process parameters did not result in control of the iron content in the cobalt-based alloy coatings. This is because of factors governing the dilution of iron, which are varied and complex, involving various physical phenomena, such as the lasering time, or fluidic phenomena following the movement of the melt. The dilution of iron atoms and the transport of material could be due to the movement of the melt fluid (Marangoni effect) during the laser scan. This effect has been studied in the literature and is found to be important for the SLM process [17]. It was therefore decided to switch to another parameter, namely the number of layers for constant SLM parameters, in order to vary the amount of diluted iron atoms in the cobalt-based alloy coatings.

Table 1 SLM parameters used to build Cobalt-based coatings on steel substrate.

Laser Power P (W)	Scan speed v (mm/s)	Layer thickness h (μm)	Rotation angle θ	Hatching d (μm)	Temperature of the plate °C
<275	800	50	60°	120	100°

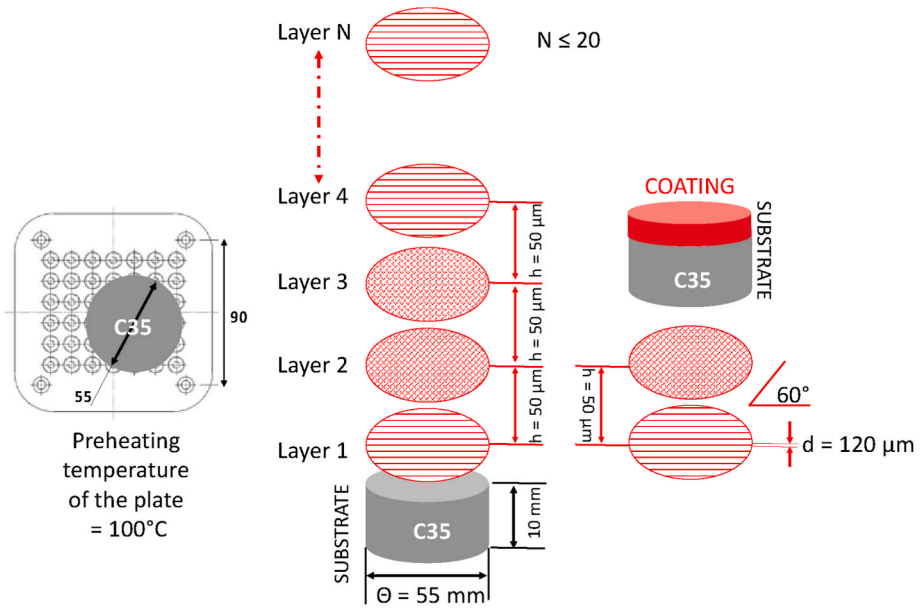

Fig. 1. SLM device and strategy for formation of the coatings on the C35 steel substrate.

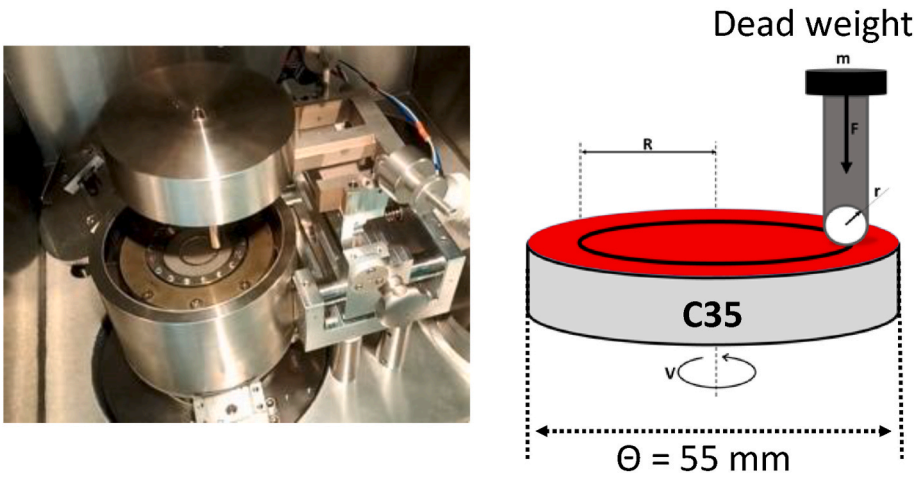

Fig. 2. Side view of the ball-on-disc type CSM Instruments tribometer.

Table 2
Tribological tests parameters (the samples of batches 1 &2 are described in Fig. 6).

	FN normal load	R Wear track radius	V sliding speed	Ω rotationnal speed	L Sliding distance	
	N	mm	mm/s	rpm	Number of laps	m
Batch 1	30	14,2	372,0	14,5	20897	2500
Batch 2	30	19,1	500,0	14,5	20897	1870

Two manufacturing campaigns (batches) were carried out to produce the cobalt-based alloy coatings with different numbers of layers on C35 steel discs. In each campaign, the disc was screwed onto the manufacturing plate and the samples were made one by one to ensure a time interval of 34 s between each layer (Fig. 1). The SLM manufacturing parameters of the CoCrMo layers are shown in Table 1. They are those recommended by the manufacturer of the machine used by SLM Solutions, except for the rotation angle, which was set at 60°.

3. Materials and characterizations

3.1. Materials

The cobalt-based coatings investigated in this study were deposited onto C35 low steel plates using the SLM process. The CoCrMo powder used was a commercial product provided by SLM Solutions. The chemical composition of the powder, according to the SLM Solutions certificate, is shown in Table 3. The composition analyzed by EDS is also

Table 3
Nominal chemical composition of alloy powder used to perform the coatings.

Element	Co	Cr	Mo	Mn	Fe	Si	P	C
wt% SLM Solution Data	63.45	28.90	6.40	0.30	0.20	0.60	0.04	0.11
wt% EDS-SEM analysis	62.86	28.32	6.12	0.93	0.42	1.36	/	/

given in the same table. It can be noticed that the iron content in this powder is very low and considerably lower than 0.5% mass. The particle size was in the range of 15 and 45 μm diameter, as specified by the supplier, but most were smaller than 50 μm in diameter. For this reason, the layer thickness was 50 μm.

3.2. Measurement of the wear volume of cobalt-based alloy coatings

After ultrasonic cleaning with ethanol, the wear volume measurements of cobalt-based alloy coatings were performed by surface topography measurements using a confocal microscope (Altisurf520® from Altimet), with a chromatic confocal probe (measure range of 350 μm) and an axial resolution of 11 nm (data given by Altimet supplier). On each disc and on the wear tracks, four areas of dimensions 5 mm (10 μm step) x 3 mm (10 μm step) ($5 \times 3\ mm^2$) were scanned and then processed by the Altimap® software to extract the average wear profile. The wear volume was finally calculated by multiplying the area of the average wear profile by the circumference of the wear track. In this paper, the term "wear volume" is associated with the free particles of coatings ejected from the contact.

3.3. Hardness of the cobalt-based alloy coatings

The hardness of the different cobalt-based coatings was measured by micro-hardness filiations on cross-sections. Several filiations were performed (Vickers 200 g) and the average hardness of the coatings were then calculated, taking into account all the indentations out of the thermally affected areas (TAZ).

After tribological tests, the cobalt-based coating hardness was also measured by micro-hardness filiations on cross-sections perpendicular to the sliding direction. Vickers indentation filiations were achieved in the plastically sheared area with 25 g normal load. The set up allowed the distance between two neighboring indentations to be at least 2.5 times the size of the indentation, which meant that indentations were made diagonally in order to increase the number of prints in the coating. The first value was measured at a distance of 30 μm from the surface, because of the size of the Vickers indentations (Fig. 3).

3.4. Assessment of chemical compositions and microstructures of the cobalt-based alloy coatings

The chemical compositions were measured at the surface of the samples by EDS-SEM. Before testing, the analyses were made in one section in the center of the surface. After testing, the analyses were made in four sections of 120 μm × 25 μm at an accelerating voltage of 15 kV (Fig. 4).

TTribological wear tracks were also observed in cross-section parallel to the sliding direction. The samples are cut, mounted in an electrically conducting material (KonductoMet®), ground with 80–1200 grit paper, polished with diamond particles until 1 μm and finally etched. The microstructure was revealed by electrolytic etching with a 50 vol% hydrochloric acid and 50%vol ethanol reagent, using 0.8A of current for 20s.

3.5. Crystallographic structures of the cobalt-based alloy coatings

The crystallographic analyses were achieved by X-ray diffraction (XRD) and electron backscatter diffraction (EBSD) techniques. Before the tests, XRD analyses were performed on top surface of the coatings to obtain a global measurement of the crystallographic phases (Fig. 4). After the tests, DRX measurement analyses were performed on 2 dia-metrically opposed areas. Classical θ-θ measurements and pole figure measurements were made using a PANalytical X'Pert Pro diffractometer with a cobalt anticathode ($\lambda K\alpha 1 = 1{,}789$ Å), with an iron filter to limit the fluorescence effect of the cobalt.

In this work, the EBSD technique was used to refine the XRD results with a focalization on the gradients of microstructural modifications of FCC phase into HCP phase transformations on the 100 first micrometers under the sliding surface. This techniquewas also used to characterize the texturing of the grains in the plastically deformed areas under the action of shear, and to identify the thickness of the plasticity-induced phase transformation.

The EBSD analyzes were performed on cross-sections parallel to the sliding direction (Fig. 5). The scanning electron microscope used for this technique was the JOEL JSM-7100TTLS LV, which is an FEG field effect microscope equipped with an EBSD detector (Nordlys Nano, Oxford Instruments). It is composed of a phosphorescent screen and a CCD camera that allows the automatic capture and processing of diffraction images (AZtec software, Oxford Instruments). The surface preparation is rather complex because the studied surface implies polishing a bi- material (substrate + coating) with a very thin coating thickness. An ion etch polishing called "CrossPolisher" was used because ion etching is the most suitable technique to obtain a clean surface, so as to observe the extreme surface of a sample in section while avoiding work-hardening due to sample preparation. In this study, a JEOL model IB-19510CP Argon Ion Mill Cross-section polisher device was used. The accelera-tion tension was 6 KV with 4 h duration. A view camera was integrated to follow the ionic polishing.

With these analyses, only the results of two samples (1st batch) will be presented.

- A 10-layer coating (with an average thickness of around 385 ± 35 μm) and a surface iron content by mass of around 9%. The initial phase is a FCC phase. The phase transformation after tribological testing, observed by XRD, will be a complete FCC to HC phase.
- A 4-layer coating (average thickness around 238 ± 4 μm) and a surface iron content by mass of around 65%. The initial phases are

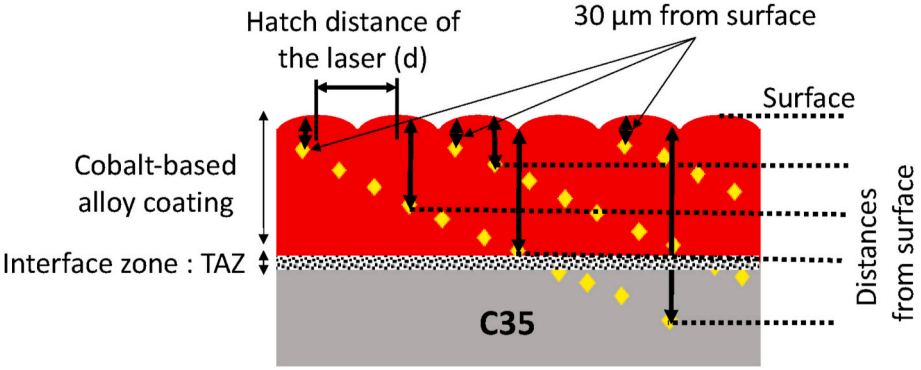

Fig. 3. Schema of the Vickers microhardness filiations (cross-section) in the cobalt-based coating.

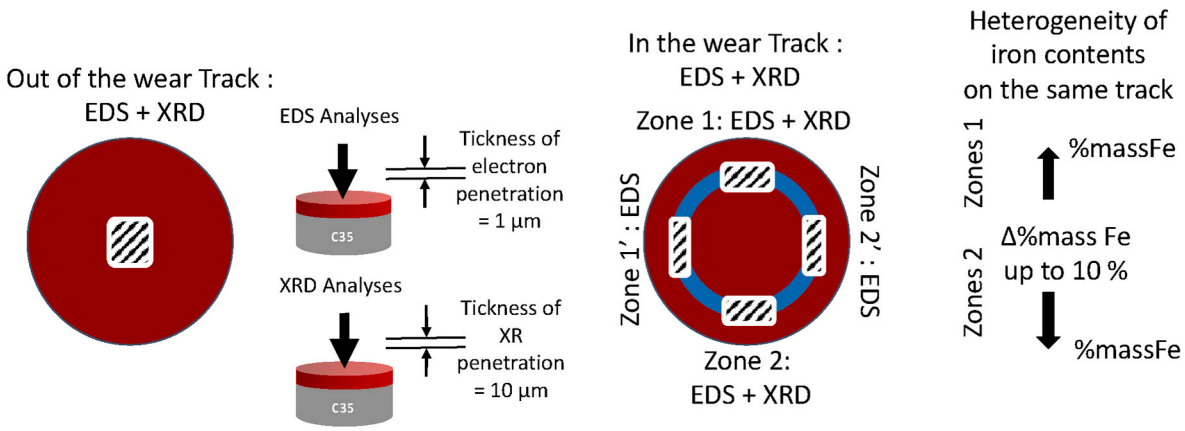

Fig. 4. Location of EDS-SEM and XRD analysis areas on the coating before and after tribological testing at the surfaces of the coatings.

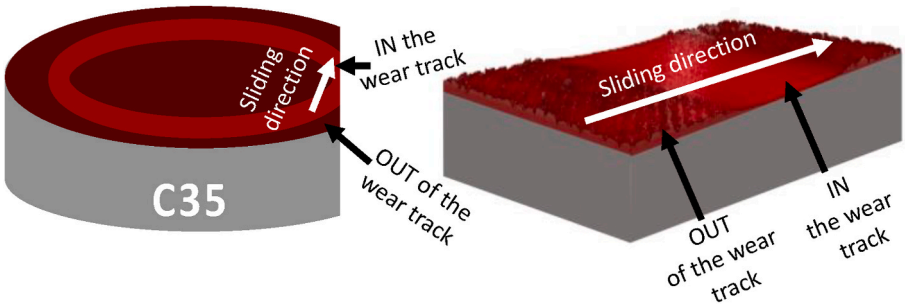

Fig. 5. Schema of locations of electron backscatter diffraction (EBSD) analyses.

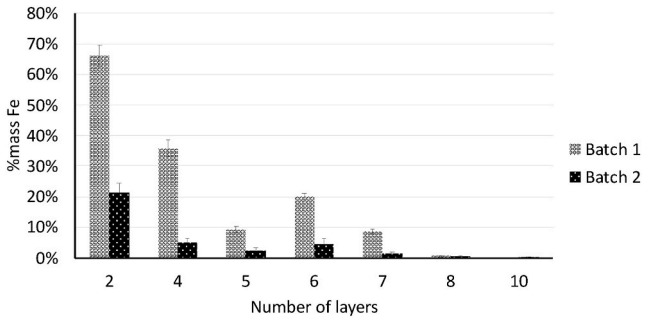

Fig. 6. Values of Iron content (%mass Fe) versus the number of layers measured by EDS-SEM at surfaces of the cobalt-based coatings.

FCC plus α′-BCC phases. The phase transformation after tribological testing would be of the form FCC + α′BCC → α′BCC.

The measurement step was 1 µm for all cases. The acquisition frequency was 20.38 Hz for the 10-layer case and 66.30 Hz and 40.03 Hz respectively for the 4-layer case for the areas outside and inside the wear track.

4. Results

4.1. Cobalt based alloy coatings before tribological solicitations

4.1.1. Iron contents and crystalline phases in cobalt based alloy coatings

For the two manufacturing campaigns or batches, the surface iron mass content (%mass Fe), identified by EDS-SEM analyses, decreased with the number of layers (Fig. 6). A great difference of iron content was observed between the two batches. It should be noted that the two were spaced out in time (8 months). The two production runs were carried out under the same conditions, but with several months between them, with one maintenance operation carried out in that time during which the argon flow rate was changed from 6.32 m/s to 4.14 m/s. At this step of the study, we are not able to give a real explanation for this difference of iron content in the coatings depending on the number of layers.

In this work, this discrepancy should not be considered as a scientific problem as this study concerns the relationship between the iron content of cobalt-based alloy coatings and their plastic mechanical behavior under tribological loads, independently of the number of coating layers. For this reason, in the following, the tribological results will be presented mainly as a function of the iron content of the friction surface and not as a function of the number of layers used to produce the coating.

Fig. 7 presents the amount of crystalline phases (% Phase) versus the iron mass content (diluted %mass Fe) identified at the surface of the coatings by XRD analyses before tribological tests. In this graph, all the

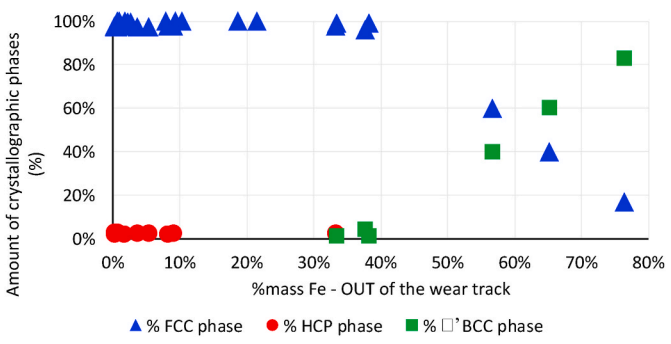

Fig. 7. Amount of crystalline phases (XRD Analyses) versus the surface mass iron content (EDS-SEM) identified at the surface of the coatings before tribological tests.

results of the two batches are compiled. Regardless of the average mass content of iron, a metastable FCC phase was identified. An HCP phase was observed in very small quantities (<3%) for iron contents lower than 32% by mass. This could be the result of a relatively short cooling time and low iron content, or a phase transformation due to internal stresses during cooling. The α′-BCC phase only appears for iron mass contents above 33% mass (in this case 33.43%). The amount of α′-BCC phase increases from 40% to 60% for iron contents between 55 and 65% and reaches 83% for an iron content equal to 76%. In the following, we will note α′-BCC, the Cubic-Centered phase of iron, identified in XRD but whose hardness is around 700HV. High iron contents and rapid cooling lead to the formation of martensite α′-BCC and not ferrite BCC.

The high level of dilution of iron in some coatings initially performed from cobalt-based powder suggests that the tribological behavior could more related to an iron-based system than a cobalt-based system.

4.1.2. *Cobalt based alloy coating hardness*

Fig. 8 shows the evolution of the average value of hardness (HV0,2) of the cobalt-based alloy coatings versus the iron mass content (diluted %mass Fe). The values are averaged over the entire thickness of the coating excluding the Thermally Affected Zone. This result is provided from a previous study focused on microstructural aspects of cobalt-based alloy coatings [18]. The hardness of the substrate is 190 ± 20 HV0,2 and the hardness of the cobalt-based alloy coating without diluted iron is around 409 ± 31 HV0,2.

The hardness decreases when diluted iron increases in the cobalt-based alloy until a minimum value of 32% mass iron, before increasing again until reaching a maximum for 69% mass iron. Up to 32% mass iron, the display of iron in solid solution in the metastable FCC phase of the cobalt-based alloy softens the coating. Above 32% mass iron, martensite α′-BCC is formed, which increases the average hardness of the alloy. The α′-BCC martensitic phase is proved with more than 80% mass iron. The cobalt-based alloy coating is very hard with a hardness of more than 600HV. In this case, about it is more a case of iron-based alloy coating rather than cobalt-based alloy coating.

4.1.3. *Crystalline phases analyzed by EBSD in cross sections*

To improve the classical tribological results by identifying the microstructural evolutions in the cobalt-based coating observed by standard methods (DRX, EDS, …) under tribological stresses, EBSD analyses were carried out on two samples. These analyses were performed to understand some plastic mechanisms that take place at the grain scale in the coatings. We carried out EBSD mapping of the coatings in cross-sections, which allowed the microstructure to be observed, including the grain boundaries, which are not observable by chemical etching. The joints of the melting baths were also highlighted.

The images in Fig. 9 show the phases and the crystallographic orientations of the grains around the X-axis using the RGB color code, for both types of samples.

For 10-layer coating iron (~9% average surface iron mass), the grains are columnar, and one grain can pass through several layers. This is called epitaxial growth in additive manufacturing (Fig. 9-a). The grain sizes vary between 4 μm and 104 μm. We note the presence of a grain boundary that runs through the entire thickness of the coating in the middle of each laser pass. According to our image analysis estimations, the grain growth direction is about 46° ± 10° with respect to the manufacturing direction.

In the case of the 4-layer coating (~61% average surface iron mass), a large number of grains are more or less equiaxed in shape and smaller in diameter (<21 μm) (Fig. 9-b). This could be the result of a relatively homogeneous cooling in the thickness of the coating. The thermal gradient in the coating thickness could be lower than it would be in a thicker coating, and for which columnar grains are observed [19]. The orientation of the grains is random throughout the section observed, but for the largest grains, we find more or less the same orientation as for 10 layers.

In addition, for the 10-layer coating, equiaxed morphology grains are observed at the coating/substrate interface which corresponds to the Thermally Affected Zone. Considering this observation, we can make a very strong assumption that in the 4-layer case, the full thickness of the coating presents the same features as the heat affected zone.

On the phase maps of Fig. 10, the crystallographic phases of the two coatings are presented. The 10-layer coating is predominantly a single- phase FCC system throughout the thickness of the coating with residual HCP phase at the extreme surface (Fig. 10-a). The 4-layer coating cor-responds to a two-phase α′-BCC + FCC system throughout the thickness of the coating (Fig. 10-b), which corroborates the high values of micro- hardness. The α′-BCC phase is largely in the majority in the coating thickness and the FCC phase is mostly observed in the melt joints constituting the interface between the laser passes. The calculation of the phase amount with the EBSD method shows a ratio (%FCC phase/ %α′-BCC phase) of 10/90 in favor of α′-BCC phase inside the coating, while at the extreme surface this ratio is 38/62, still in favor of the α′-BCC phase. The latter ratio value is close to that measured by XRD, which gives 40/60 in favor of the α′-BCC phase.

4.2. *Cobalt-based alloy coatings under tribological sollicitations*

4.2.1. *Iron contents and crystalline phases in cobalt-based alloy coatings*

After tribological tests, the iron content is higher in the wear track than outside the wear track for the discs of the two batches (Fig. 11). The same study as previously mentioned, focused on the microstructural aspects of Cobalt-based alloy coatings [18], shows a slight increase in the evolution of the diluted iron content in the thickness of the coating from the external surface to the interface. Our result is therefore consistent, since the source of iron dilution is the substrate/coating

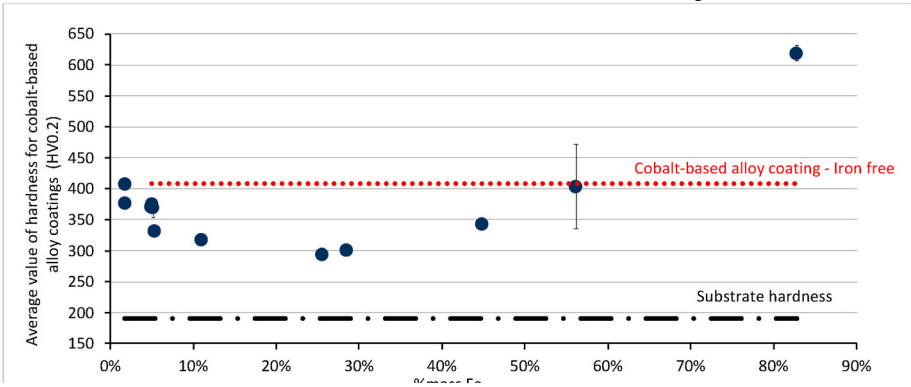

Fig. 8. Evolution of the average value of hardness of the cobalt-based alloy coatings versus the surface mass iron content.

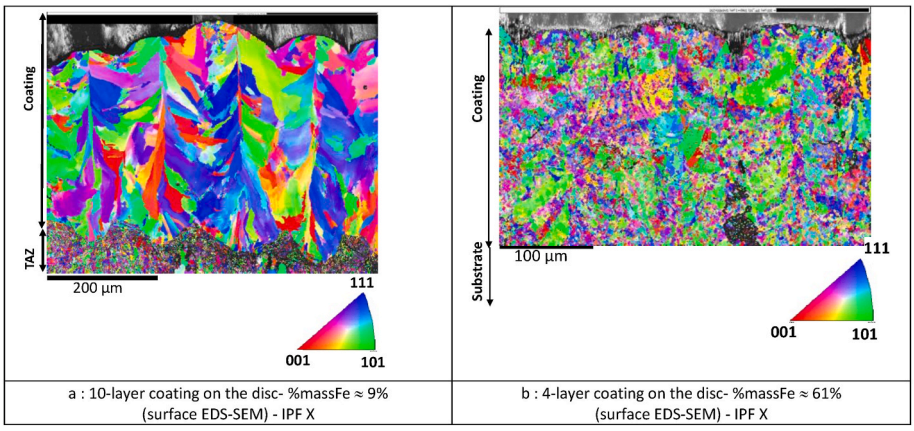

a : 10-layer coating on the disc- %massFe ≈ 9% (surface EDS-SEM) - IPF X

b : 4-layer coating on the disc- %massFe ≈ 61% (surface EDS-SEM) - IPF X

Fig. 9. IPF X orientation maps for the 10-layer and 4-layer coatings outside the wear track.

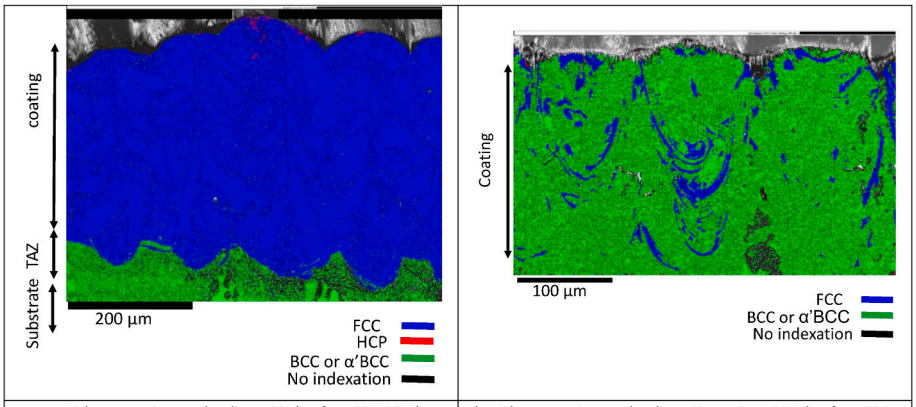

a : 10-layer coating on the disc ≈ 9% (surface EDS-SEM)

b : 4-layer coating on the disc - %massFe ≈ 61% (surface EDS-SEM)

Fig. 10. IPF X orientation maps for the 10-layer and 4-layer coatings outside the wear track.

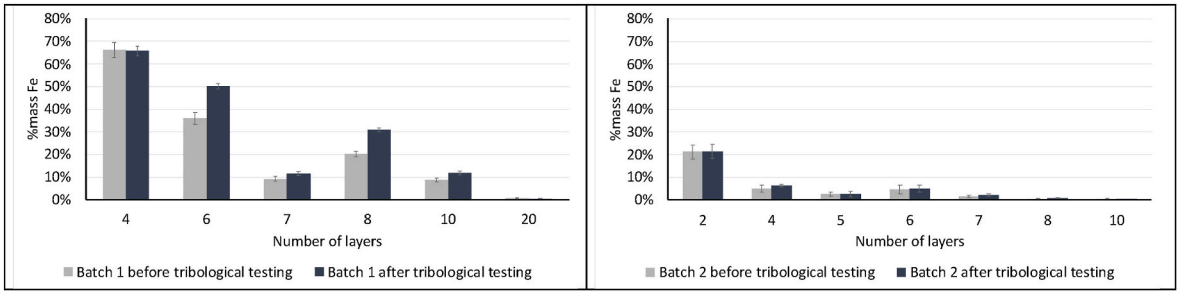

Fig. 11. Values of Iron content (%mass Fe) versus the number of layers measured by EDS-SEM at surfaces of the cobalt-based coatings before and after tribological tests.

interface, and with wear this interface tends to be reached. Overall, the variation in iron mass content versus the number of coating layers is the same after tribological testing as that observed before testing.

Fig. 12 shows the amount of the three crystallographic phases (FCC, HCP and α′-BCC phases) versus the % mass of diluted iron at the surface of the wear tracks. Fig. 12 has to be compared with Fig. 7. For iron mass contents below 33% at the surface of the wear track, the phase becomes entirely Hexagonal Compact (HCP). So, with the tribological conditions used in the tests, the phase transformation FCC into HC phase is complete.

When the iron mass content in the wear track is between 48.8% and 52% mass, presence of FCC crystalline phase is always observed, but α′-BCC crystalline phase appears. The amount of the FCC crystalline phase is slightly higher than the α′-BCC phase. An exception is for 48.8% mass iron where the three phases are observed.

For iron content higher than 65% mass, only crystalline α ′-BCC phase is observed at the surface of the wear track. In this case, the interpretation is that the entire amount of the metastable FCC phase which was initially present at the surface of these cobalt-based coatings is completely transformed into α′-BCC phase under tribological stresses.

4.2.2. Friction coefficients and trends

The tribological behavior was assessed with two parameters which are the averaged values of the friction coefficient over the whole test duration versus the iron content (%mass Fe) at the surface of the wear track (Fig. 13) and the worn volumes (Fig. 15). As previously, the results

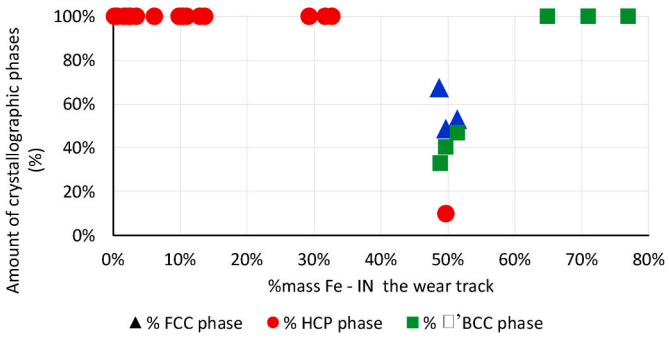

Fig. 12. Amount (%) of the crystallographic phases (FCC, HCP and α′-BCC phases) versus the %mass iron at the surface of the wear tracks.

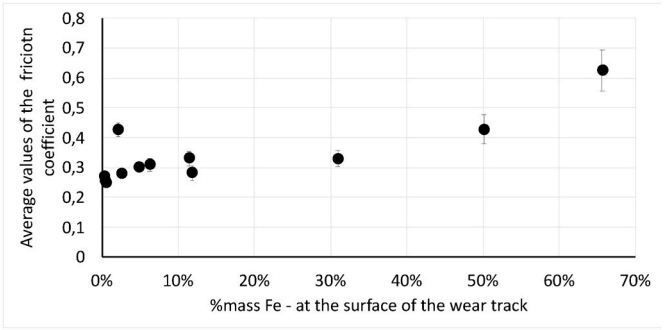

Fig. 13. Evolution of the average coefficient of friction as a function of the iron content at the surface of the wear track for all fabrications.

are given by compiling the results of the two batches.

In Fig. 13, it is shown that between 5% and 32% mass iron, the average value of the friction coefficient versus the mass iron content at the surface of the wear track is almost constant (of the order of 0.3). Below 5% mass iron, the friction coefficient is globally lower than 0.3. Above that, it increases significantly to reach a value over 0.6 for 68% mass iron by mass.

To get a better understanding of the evolutions of the average values of friction coefficients versus the mass iron content at the surface of the wear track, Fig. 14 shows the recordings of the friction coefficient curves as a function of sliding distance for two illustrative cases: the test with a 4-layer (1st batch) coating on the disc and the test with a 10-layer (1st batch) coating on the disc. When the iron content is high in the cobalt- based alloy coating (above 30% by mass), the evolution of the friction coefficient as a function of the sliding distance shows high values (above 0.6), with large instabilities of friction at the end of the test. These are generated by the circulation of wear debris in the contact. When the iron content is low (less than 10% by mass), the evolution of the friction coefficient as a function of the sliding distance shows low values (less

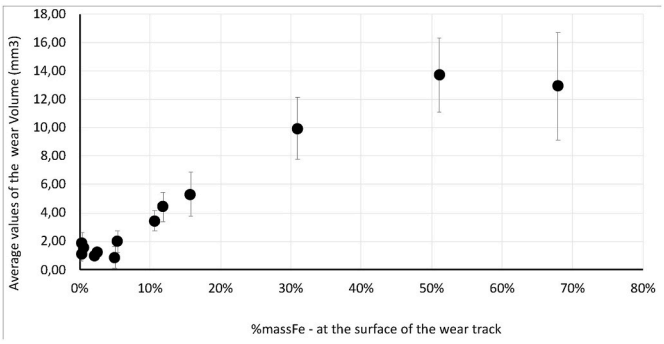

Fig. 15. Evolution of the wear volume versus the iron content (%mass Fe) in the wear track for all tribological tests.

than 0.2) and no instabilities of friction is observed. The evolutions of the friction coefficient are in relation to the contact surface evolutions, as debris circulation but also as crystallographic transformations.

4.2.3. *Wear volumes of cobalt-based alloy coatings*

Table 4 and Fig. 15 show the evolution of the wear volume (mm^3) of the coated discs as a function of the mass iron content at the surface of the wear track. For mass iron contents below 10%, the wear volume is weak, almost constant, and less than 3 mm^3. The wear volume increases for mass iron values between 10% and 30% and finally stabilizes at 10 mm^3 for values above 50% mass iron.

Considering all the tests, the wear depth is almost constant (around 50 μm for iron mass contents over 20%), while it is the width of the wear track that evolves very significantly in relation to the iron content, evolving in the same way as the wear volume. The purpose of this study is to determine the influence of the plastic deformation accommodation mechanisms on tribological behavior by studying the effect of the iron content in cobalt-based alloys. For this reason, the discussion of the results will be not focused on the interpretation of the levels of the wear rates, even these values are high.

4.2.4. *Hardness evolution of damaged cobalt-based alloy coating surfaces*

Friction leads to damage of cobalt-based alloy coating surfaces by local plastic strain. While plasticity can be assessed by phase transformations, it is also assessed by the level of work or strain hardening, which is the result of dislocation entanglement, also causingthe increase in hardness. Plastic strain can be observed with the grain reorientation in the direction of the frictional forces. As the coatings are performed by an SLM process, we note that the most easily observed feature under microscopy will be the reorientation of the melt joint and not the grain joint itself.

Fig. 16 plots the hardness evolutions of the cobalt-based alloy coatings of the tribological test disc as a function of their thickness, for two illustrative cases: the 4-layer and 10-layer coatings. For the case of the 4- layer (1st batch) coating, the content of the diluted iron is high (around

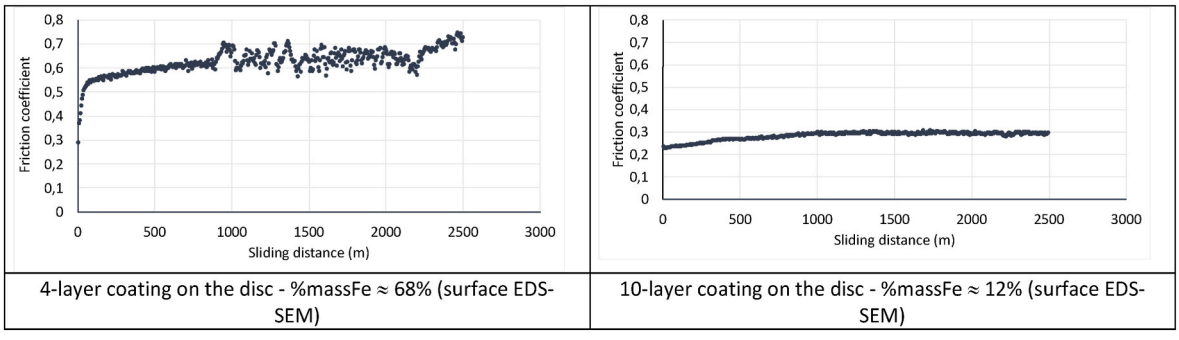

Fig. 14. Evolution of the coefficient of friction versus sliding distance for two cases (4-layer & 10-layer- batch1).

Table 4
Compilation of all the tribological results including calculations of the wear volumes and wear rates.

	Number of layers	Sample reference	Average value of %massFe, at the surface of the wear track	StdDev	Average value of %massFe, out the surface of the wear track	StdDev	Average value of the friction coefficient during the tests	StdDev	Average wear volume mm^3	StdDev	Average wear rate $mm^3/N.m$	StdDev
1rst batch	4	D1.2	67,93%	0,03	60,94%	0,04	0,625	0067	12,92	3,82	1,72E-04	5,10E-05
	6	D2.1	51,07%	0,02	37,39%	0,04	0,428	0048	13,71	2,62	1,83E-04	3,49E-05
	8	D3.1	30,96%	0,02	20,11%	0,01	0,329	0028	9,95	2,21	1,33E-04	2,95E-05
	10	F2.1	11,85%	0,02	9,25%	0,01	0,281	0026	4,45	1,03	5,93E-05	1,37E-06
	7	F1.1	10,66%	0,02	8,50%	0,01	0,331	0024	3,44	0,73	4,59E-05	9,67E-06
	20	F3.1	0,37%	0,00	0,65%	0,00	0,256	0014	1,84	0,75	2,46E-05	1,00E-05
2^{nd} Batch	2	H7.1	15,74%	0,08	12,46%	0,07	0,576	0078	5,32	1,57	7,09E-05	2,09E-05
	4	H2.1	5,37%	0,04	4,92%	0,03	0,309	0021	1,98	0,75	3,54E-05	1,34E-05
	5	H6.1	2,57%	0,01	2,43%	0,01	0,279	0013	1,21	0,31	2,17E-05	5,61E-06
	6	H3.1	4,99%	0,02	4,07%	0,02	0,301	0012	0,87	0,07	1,56E-05	1,36E-06
	7	H1.1	2,11%	0,01	0,00%	0,01	0,425	0023	0,95	0,07	1,70E-05	1,23E-06
	8	H4.1	0,58%	0,00	0,44%	0,00	0,247	0009	1,53	0,42	2,73E-05	7,49E-06
	10	H5.1	0,27%	0,00	0,25%	0,00	0,271	0011	1,07	0,48	1,91E-05	8,64E-06

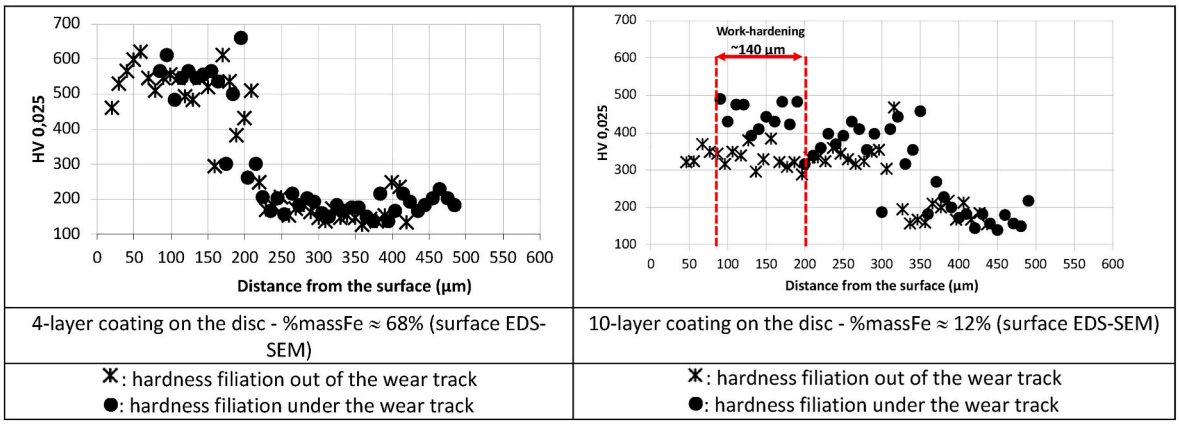

Fig. 16. Evolution of the micro-hardness versus distance from coating surface for two cases (4 layers & 10 layers).

68% in mass) and the EDS-SEM surface analyses display two crystalline phases, with α′-BCC and FCC phase grains. Whereas, for the case 10-layer (1st batch) coating, the content of the diluted iron is low, at around 12% in mass, and EDS-SEM surface analyze gives only a FCC crystallographic phase.

The measurements were made from the surface of the coating towards the bulk substrate from cross-sections perpendicular to the direction of friction. We carried out only two filiations per sample (one out of the friction zone and one under the worn track, at the center) and the load applied was 25 g. The filiation under the wear track is shifted by a distance equal to the average depth of the wear track, previously evaluated by profilometry with the Altisurf520® device.

The results of hardness evolution, out of the wear track (cross marks), confirm that the higher the diluted iron content (4-layer coating), the higher the hardness of the cobalt-based alloy coating, due to a large amount of α′-BCC crystallographic phase in the grains. In this case, the chemical composition of the coating is a mixture of iron of the substrate and elements of the powder, with a predominance of iron. Inversely, for low diluted iron content (10-layer coating), the hardness is low, and lower than free iron cobalt-based alloy coating.

The results of the hardness evolution tests, in the wear track (disc marks), show that there is no real increase in hardness for the diluted high-iron coating (4-layer coating) but there is an increase in hardness for the diluted low-iron coating (10-layer coating). In the case of 10-layer coating, the thickness of work-hardening is estimated to be about 140 µm.

Under tribological stresses, a reorientation of the melt joints in cross section of the coating, parallel to the direction of sliding is observed. The thickness affected by this reorientation was evaluated by SEM observation. It was noted that the thickness affected by the tribological stress estimated by the reorientation of the joint was lower than that estimated by the hardness filiation measurements. For example, in the case with 12% iron corresponding to the 10-layer case (Fig. 17), the estimated affected thickness due to the reorientation of the melt joint is of the order of 23 µm, while the micro-hardness measurements showed an increase in hardness over a thickness of 140 µm (Fig. 16).

To try to quantify the work-hardening after friction tests, we assessed a value of the work-hardening rate versus the iron content in the coatings. The work-hardening rate was calculated (equation 1) after superimposing the two filiations, on the estimated work hardened thickness of the coatings, i.e. several tens of micrometers. Care was taken not to consider the hardness values of the TAZ in the calculation of the work-hardened thickness.

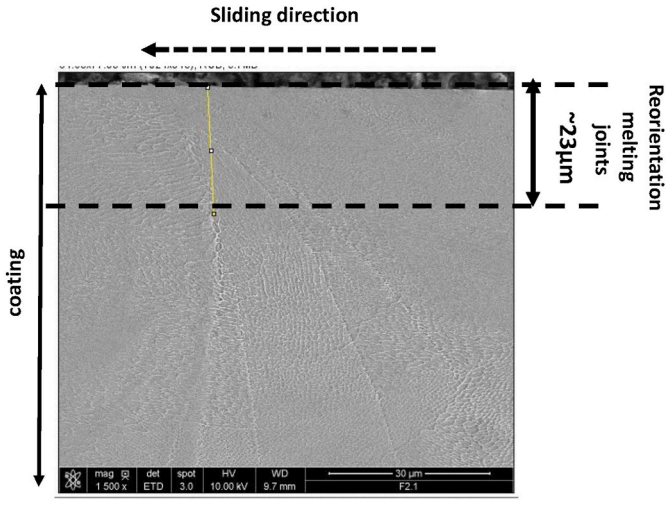

Fig. 17. SEM cross section of the 10-layer coating: reorientation of the melt joints.

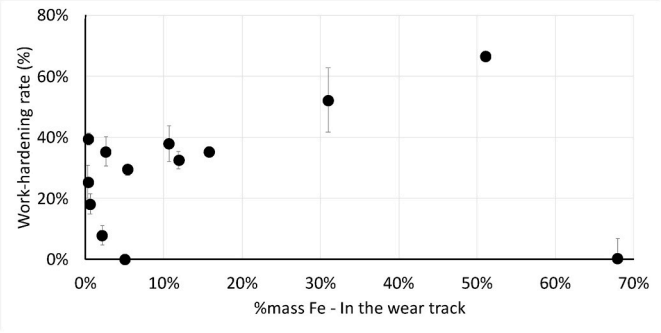

Fig. 18. Evolution of the work-hardening versus the iron content at the surface of the cobalt-based alloy after tribological tests.

$$\text{Work} - \text{hardening rate } (\%) = \frac{H_v(\text{mean value in the wear track}) - H_v(\text{mean value out of the wear track})}{H_v(\text{mean value out of the wear track})}$$

Fig. 18 shows work-hardening rates versus the mass content of iron in the wear track. Three trends are observable.

- In the range of iron contents below 10% by mass, the work-hardening rate corresponds to a scatter plot and no trend is notable. But, if we eliminate the two points below 10% of work-hardening rate, the values could show a linearity trend.
- For an iron content up to 55% by mass, the strain hardening rate varies linearly.
- For high value of iron content (65%), there is no further work-hardening rate

4.2.5. Crystalline phases analyzed by EBSD in cross sections and comparisons

Figs. 19 and 20 show the crystallogaphic modifications of the cobalt- based alloyed coatings for the two illustrative cases. Considering the wear depth loss, each figure displays cross sections of the worn track (right part). Crystallogaphic modifications are observed in the tribo-logical transformed areas below the wear track for both coating thicknesses.

For 10-layer coatings (Fig. 19), non-indexed points can be spotted at the extreme surface of the worn area (the first 20 μm thickness). Ex-planations for these non-indexed points could be the manifestation of high dislocation density, or nanometric sized grains. Just below this zone, the initial crystallographic system has been completely trans-formed from a single-phase FCC system to an HCP phase microstructure. Below this, for a further 120 μm, the phase transformation is not com-plete and there is a mixture between the FCC phase and the new HCP phase. The amount of the HCP phase decreases with the thickness of the coating. Finally, in the last 100 μm of the coating thickness, the crys-tallographic system remains in the FCC metastable phase, as before any tribological test.

For the 4-layer coating (Fig. 20), the transformation of the FCC phase to a α′-BCC phase is highlighted in the melt joints, and this trans-formation is complete over the whole thickness of the coating. Only a blue trace of residual FCC phase is observed. So, under friction sol-licitations, the system evolves from a two-phase BCC+α′-BCC phases towards a completely α′-BCC phase microstructure. Thus, the FCC phase to α′-BCC martensite phase transformation seems to take place from the coating surface to the substrate/coating interface, i.e. over ~150 μm. Moreover, contrary to the case of the 10-layer coating, no non-indexed zones (black zones) are observed.

Using the Aztec software features, EDS-SEM measurements (cross marks) were carried out in FCC and α′-BCC grains (Fig. 21). In the unworn surface side (out of the wear track) and for all analyzed areas, the iron mass content is lower in the FCC grains than in the α′-BCC grains. It increases in the α′-BCC grains from the surface of the coating (60.28% ± 2.74% by mass) towards the substrate/coating interface (74.83% ± 15.82% by mass), whereas in the FCC grains it is almost constant (~47% mass), although it becomes slightly higher at the substrate/coating interface (50.72% ± 7.81% by mass). Considering these analyses, the average values of iron mass contents in the FCC grains vary from ~41% to ~51%, and in the range of ~61%–~75% by mass in the α′-BCC grains.

In the worn area, the iron mass content analyses in the α′-BCC phase grains show two trends with different iron mass contents. The first trend has mass contents of between ~80% and ~88% (direction ↗of the arrow), preferentially in relation to the contents in the α′-BCC phase of the unworn coating. The second trend has iron contents ranging from ~50% to ~60% by mass (direction ↘of the arrow). These areas are heterogeneously distributed through the thickness of the coating, where FCC phase grains were initially present in the melt joints. This information suggests that these regions corresponded to initial FCC phase grains which have been transformed into α′-BCC under tribological stresses. These results complement and support the hypothesis of an FCC into α'-BCC transformation under tribological stresses.

5. Discussion

This work is focused on the mechanism of plasticity accommodation in tribological sub-surfaces under frictional loads. Under tribological loadings, metallic surfaces could accommodate velocity and loading by formation of Tribologically Transformed Surfaces. Tribologically Transformed Surfaces (TTS) or Mechanically Modified Superficial (MMS) structures are the results of changes in the microstructural features, chemical composition and mechanical and thermal properties of ductile materials submitted to large plastic deformations under high hydrostatic pressures, even at low temperatures [20–22]. The TTS are linked to high sub-surface plastic strains and the TTS thickness depends on both material properties and tribological test conditions.

The results presented in this paper focus on crystallographic transformations and work-hardening in cobalt-based alloy coatings under tribological shear stresses. In this case, the phase transformations, as well the work-hardening, are dependent on the amount of diluted iron in the coatings, which influences the plasticity mechanisms of the TTS and

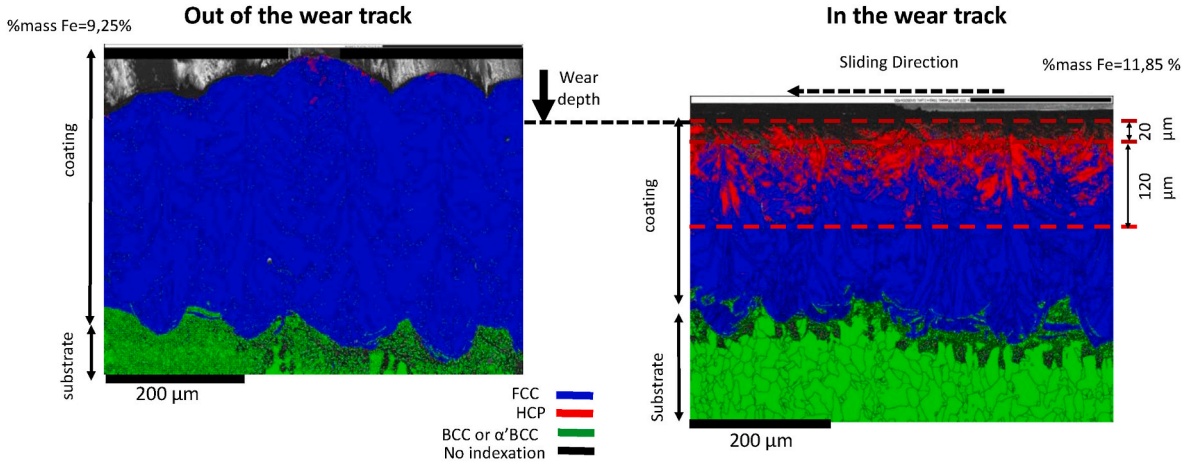

Fig. 19. Crystallographic modifications of the cobalt-based alloyed coatings for the case 10-layer coating - %massFe = 12%.

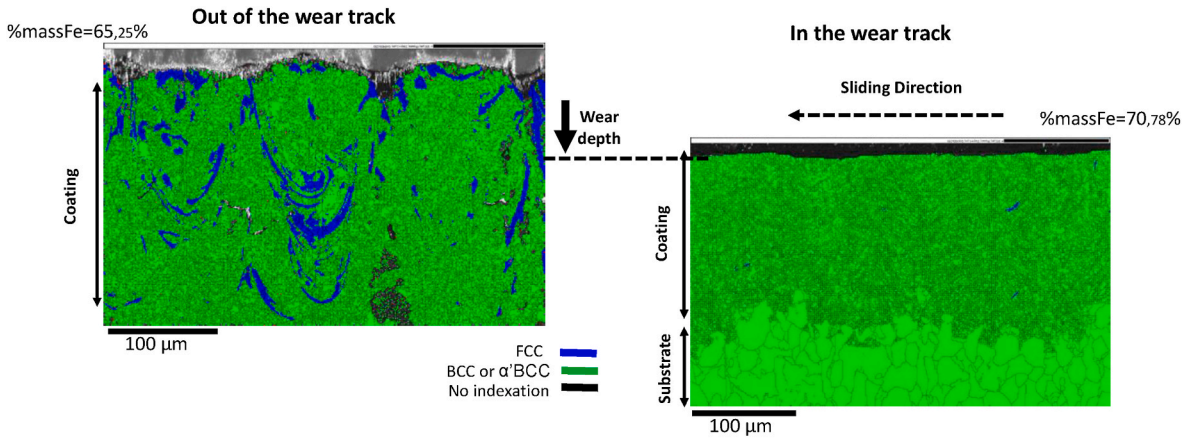

Fig. 20. Crystallographic modifications of the cobalt-based alloyed coatings for the case 4- layer coating - %massFe = 68%.

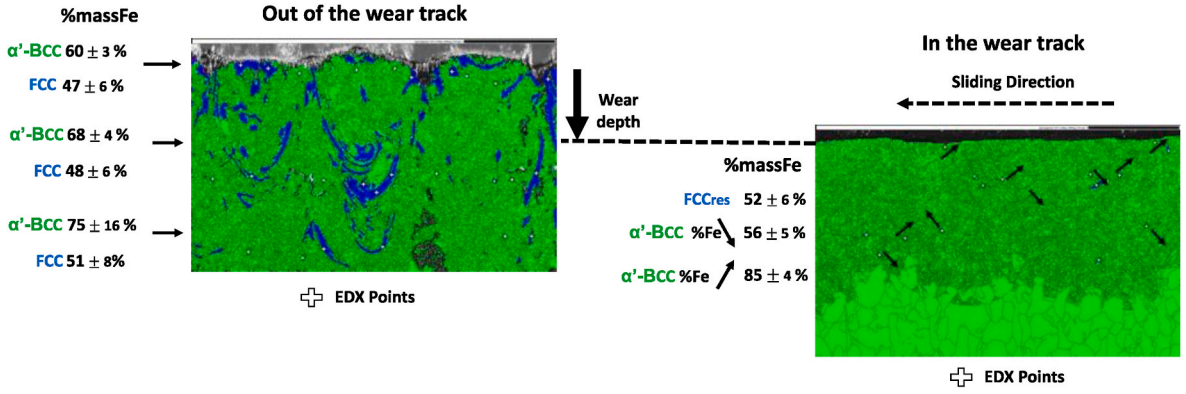

Fig. 21. Iron mass contents measured by EDS-SEM in each of the FCC and α′-BCC phases out of the wear track and in the wear track for the 4-layer case.

thus the behaviour of the friction surfaces. The high level of dilution of iron in coatings initially performed from cobalt-based powder suggests that the tribological behavior could be more related to an iron-based system than a cobalt-based system. This could be true for coatings with a low number of layers, such as the 4-layer coating, where the iron content is around 61% by mass before tribolgical testing.

In this case, we assume that the crystallographic transformations are only explained by the plasticity shear induced by tribological stresses, as shown by Hou et al. [4] and Cabrol et al. [3,23] for the FCC phase into HCP phase transformation and Lee et al. [24] for the FCC into α′-BCC transformation. It is validated in the literature that iron stabilizes the metastable FCC phase in cobalt-based alloys, thereby decreasing the charge density in the stacking fault regions. Iron increases the energy of stacking faults in these alloys, which reduces the formation of partial dislocations and thus delays the metastable FCC into HCP phase change [1,9,10].

The results show that before tribological tests, two different crystallographic systems are present depending on the iron content. For low iron contents, single-phase cobalt-based coatings with an FCC initial phase are found. For high iron contents, two-phase cobalt-based coatings, consisting of FCC and α′-BCC phases, are observed.

Under tribological sollicitations, cobalt-based alloy coatings act like a cobalt-based coating up to ~33% iron mass and the transformation of the FCC phase to the HCP phase is complete at the coating surface. Above 50% (48.80%) mass iron, the FCC phase transforms into α′-BCC martensite and this transformation is significant when the cobalt-based alloy coating is rich in iron and poor in cobalt elements (from 65% mass iron, the transformation of the FCC phase into α′-BCC is complete). The cobalt-based alloy then behaves more like an austenitic steel. Between these two limits - 33% and 50% - we have a mixed system, for which it is difficult to determine the amount of transformation of the FCC phase into HCP or α′-BCC phases. It remains difficult to determine the rate of plasticity-induced transformation into α′-BCC or HCP phases.

The results show that a total phase transformation is limited in thickness. We therefore assess that the iron content (and thus indirectly the thickness of the coating), the grain morphologies, the nature of the phase transformation and the quantity of phase to transform are parameters that condition the thicknesses affected by the phase transformations induced by plasticity under such tribological conditions.

When the coating thickness is of the order of 385 µm for the 10-layer case, EBSD coating measurements show that the thickness for which the FCC into HCP transformation is complete is the first 20 µm. A further 120 µm of partial phase transformation can be noted. In addition, the hardness filiation curves showed an increase in hardness over a thickness of about 140 µm, revealing a work-hardening effect in addition to phase transformation. From these results, it is strongly assumed that when the transformation occurs in one large grain, a "domino" effect may occur and lead to the phase transformation of the whole grain (Fig. 19).

For thinner cobalt-based coatings with a high iron content (4-layer

coating with 205 ± 21 μm thickness), the entire thickness of the coating is affected by the FCC into α′-BCC phase transformation.

So, in the case of 4-layer coating, we can observed that with grains more or less equiaxed in shape and small in diameter (<21 μm) and with a lower quantity of phase to be transformed, the plastic-strain affected zone is about 200 μm.

Measurements of the friction coefficients provided information that could be correlated with the previous findings. We note that when the plasticity mechanism is the total transformation of the metastable FCC into the HCP phase, low values of friction coefficient and low stability are found. This is the case for tribological tests with cobalt-based coatings for which iron contents is less or equal to 33% mass at the coating surface. We assume that the HCP phase contributes to lowering the friction coefficient and stabilizing its evolution over time.

In addition, the transformation of the FCC phase into the HCP phase contributes to a significant reduction in wear volumes. For cobalt-based coatings with a low iron content, the wear loss is low (Fig. 15) and the wear debris do not disturb the contact since no fluctuations of friction coefficient value are observed (Fig. 14). This statement is linked with the low adhesion behavior of a HCP microstructure in comparison with a FCC microstructure one. Studies on metal alloys indicate that hexagonal systems lead to lower coefficients of friction than cubic systems [25]. For iron contents above 33% by mass, when this transformation is annihi-lated in favor of α′-BCC transformation, an increase in the friction co-efficient is observed (Fig. 13). This increase is in good relationship with the level of iron content of the friction surfaces. For higher values of iron content (coating made of an iron based alloy instead of a cobalt based alloy), the values of the friction coefficient are close to those of steel (about 0.6 in dry contact) and the curve evolution is accompanied by very strong fluctuations after a certain distance, which would corre-spond to the significant emission of wear particles into the contact. The emission and circulation of the wear particles within the contact could contribute to the instabilities of friction. This statement is linked with the third body concept in the first steps of its formation with the detachment of the particles from the feed surfaces before trapping of all or part of these particles [21,26,27].

Considering the curve, the very rapid increase in the friction coefficient (Figure 14- 4-layers), which extends over the first tens of metres of sliding, corresponds certainly to the achievement of the FCC into α′-BCC phase transformation, which will then lead to a larger wear volume at the end of the test. This higher wear volume can be associated with the presence of the different crystallographic phases in the wear track. The low wear resistance is linked with a large amount of α′-BCC phase. The increase of wear starts at around 32% iron by mass and shows a trend that tends towards an asymptote for high values of iron content (Fig. 15).

With regard to friction coefficient and wear value evolutions (Figs. 13 and 15), it is assumed that when the iron content exceeds the threshold value of approximately 33%, the plasticity-induced phase transformation gradually switches from an FCC into an HCP transformation to an FCC into an α′-BCC transformation. When the iron content reaches the threshold of about 50% by mass, only the second transformation occurs.

Finally, work-hardening is observed only for coatings where the phase transormation of FCC into HCP is predominant. When the quantity of initial α′-BCC phase is high (40% for iron content beyond 50% in mass) the initial hardness is high. In this case, work-hardening is not observed, perhaps because the density of dislocations and their entanglement is already very high and does not allow additional work- hardening, even under tribological sollicitations.

6. Conclusion

A study was made of a cobalt-based powder coating on an unalloyed steel to clearly engage the iron dilution in the thickness of the coating. The chemical modifications of the cobalt-based coating imply different microstructures and crystallographic phases which are of great interest in the understanding of plastic deformation mechanisms under tribological stresses.

To allow iron dilution to occur, the SLM process was used. Tribological parts (discs) were used with different numbers of layers of cobalt-based powder.

In this work, according to the mass content of iron, two cases can be distinguished: the case where the coating is cobalt-based and the case where the coating can be considered as iron-based. A single-phase FCC system is obtained with iron mass contents at the surface of the coatings of up to 33%. Beyond this threshold, the martensitic phase α′-BCC begins to appear and coexists with the FCC phase. The quantity of the martensitic phase α′-BCC varies with iron mass content and becomes predominant from 60% by mass in iron. The quantity of α′-BCC phase can thus reach 83%.

Under tribological tests, performed with a ball-on-disc tribometer, phase transformations and work-hardening take place at the surface of the wear track.

Both the result of phase transformations and iron contents influence the tribological behaviour of these materials.

- From 0 to 33% by mass of iron, we observed a complete FCC phase into HCP phase transformation with low values of friction coefficient and low wear loss,
- From 33% to 50% by mass of iron, the FCC phase into α′-BCC phase transformation is engaged and coexists with the FCC phase into HCP phase transformation,
- Beyond 50% by mass, the FCC phase into α′-BCC phase transformation becomes predominant and the iron completely prevents the FCC to HC transformation,
- From 65% iron by mass, the FCC phase into α′-BCC phase transformation becomes complete. In this case, the FCC to α′-BCC phase transformation contributes to a high friction coefficient value and high wear loss.

Declaration of competing interest

The authors declare that they have no known competing financial interests or personal relationships that could have appeared to influence the work reported in this paper.

Acknowledgements

The authors thank IMT Mines Albi for its financial support.

References

[1] T.C. Sims, N.S. Stoloff, W.C. Hagel, Superalloys II, Wiley, New York, 1987, p. 141.
[2] L. Fouilland, M. El Mansori, M. Gerland, Role of welding process energy on the microstructural variations in a cobalt base superalloy hardfacing, Surf. Coating. Technol. 201 (2007) 6445–6451.
[3] E. Cabrol, C. Boher, V. Vidal, F. Rézaï-Aria, F. Touratier, Plastic strain of cobalt-based hardfacings under friction loading, Wear 330–331 (2015) 354–363, https://doi.org/10.1016/j.wear.2015.01.082.
[4] ˇ Houdková, Z. Pala, E. Smazalová, M. Vostřák, Z. Česánek, Microstructure and sliding wear properties of HVOF sprayed, laser remelted and laser clad Stellite 6 coatings, Surf. Coating. Technol. 318 (2017) 129–141, https://doi.org/10.1016/j.surfcoat.2016.09.012.
[5] V. Ocelík, U. de Oliveira, M. de Boer, et J. T. M. de Hosson, « Thick Co-based coating on cast iron by side laser cladding: analysis of processing conditions and coating properties », Surf. Coating. Technol., vol. 201, n° 12, p. 5875-5883, (mars 2007), doi: 10.1016/j.surfcoat.2006.10.044.
[6] J. Tuominen, et al., Fatigue behavior of laser clad round steel bars, J. Laser Appl. 27 (1) (2014), 012006, https://doi.org/10.2351/1.4903351.
[7] L.-Y. Tian, R. Lizárraga, H. Larsson, E. Holmström, L. Vitos, A first principles study of the stacking fault energies for fcc Co-based binary alloys, Acta Mater. 136 (2017) 215–223, https://doi.org/10.1016/j.actamat.2017.07.010.
[8] K. Osakada, History of plasticity and metal forming analysis, J. Mater. Process. Technol. 210 (2010) 1436–1454.
[9] T.L. Achmad, W. Fu, H. Chen, C. Zhang, Z.-G. Yang, First-principles calculations of generalized-stacking-fault-energy of Co-based alloys, Comput. Mater. Sci. 121 (2016) 86–96, https://doi.org/10.1016/j.commatsci.2016.04.031.

[10] T.L. Achmad, W. Fu, H. Chen, C. Zhang, Z.-G. Yang, Effects of alloying elements concentrations and temperatures on the stacking fault energies of Co-based alloys by computational thermodynamic approach and first-principles calculations, J. Alloys Compd. 694 (2017) 1265–1279, https://doi.org/10.1016/j.jallcom.2016.10.113.
[11] K. Graf, et al., Effect of dilution on the microstructure and properties of CoCrMoSi alloy coatings processed on high-carbon substrate, Mater. Res. 22 (1) (2019), https://doi.org/10.1590/1980-5373-mr-2018-0502.
[12] C.Y. Yap, et al., Review of selective laser melting: materials and applications, Appl. Phys. Rev. 2 (2015), 041101, https://doi.org/10.1063/1.4935926.
[13] Z. Luo, Y. Zhao, Efficient thermal finite element modeling of selective laser melting of Inconel 718, Comput. Mech. 65 (3) (2020) 763–787, https://doi.org/10.1007/ s00466-019-01794-0.
[14] T.V. Tarasova, A.P. Nazarov, M.V. Prokof ev, Effect of the regimes of selective laser melting on the structure and physicomechanical properties of cobalt-base superalloys, Phys. Met. Metallogr. 116 (6) (2015) 601–605, https://doi.org/10.1134/S0031918X15060101.
[15] E. Liverani, et al., Fabrication of Co–Cr–Mo endoprosthetic ankle devices by means of Selective Laser Melting (SLM), Mater. Des. 106 (2016) 60–68, https://doi.org/10.1016/j.matdes.2016.05.083.
[16] A. Takaichi, et al., Microstructures and mechanical properties of Co–29Cr–6Mo alloy fabricated by selective laser melting process for dental applications, J. Mech. Behav. Biomed. Mater. 21 (2013) 67–76, https://doi.org/10.1016/j.jmbbm.2013.01.021.
[17] Q. Chen, G. Guillemot, C.-A. Gandin, M. Bellet, Numerical modelling of the impact of energy distribution and Marangoni surface tension on track shape in selective laser melting of ceramic material, Addit. Manuf. 21 (2018) 713–723, https://doi.org/10.1016/j.addma.2018.03.003.
[18] T. Younsi, C. Boher, A. Soveja, Influence of interlayer time on the microstructural state of CoCrMo coatings applied by selective laser melting on an iron-based substrate for different numbers of layers, Mater. Today Commun. (2022), https://doi.org/10.1016/j.mtcomm.2022.103776.
[19] Y.J. Liu, Z. Liu, Y. Jiang, G.W. Wang, Y. Yang, L.C. Zhang, Gradient in microstructure and mechanical property of selective laser melted AlSi10Mg, J. Alloys Compd. 735 (2018) 1414–1421, https://doi.org/10.1016/j.jallcom.2017.11.020.
[20] A. Eleöd, F. Oucherif, J. Devecz, Y. Berthier, Conception of numerical and experimental tools for study of the tribological transformation of surface (TTS), in: D. Dowson (Ed.), Lubrication at the Frontier, 1999, pp. 673–682.
[21] Y. Berthier, Experimental evidence for friction and wear modeling, Wear 139 (1990) p77–p92.
[22] S. Descartes, M. Busquet, Y. Berthier, An attempt to produce ex situ TTS to understand their mechanical formation conditions - the case of an ultra high purity iron, Wear 271 (2011) 1833–1841.
[23] E. Cabrol, C. Boher, V. Vidal, F. Rezaï-Aria, F. Touratier, A correlation between tribological behavior and crystal structure of cobalt-based hardfacings, Wear 426–427 (2019) 996–1007, https://doi.org/10.1016/j.wear.2019.01.091.
[24] J.W. Christian, G.B. Olson, M. Cohen, Classification of displacive transformations: what is a martensitic transformation? Colloque C8, supplement au Journal de Physique 5 (1995), 111.
[25] M. Cartier, P. Kapsa, « Usure des contacts mécaniques » techniques de l'ingénieur [BM 5 065, 2001.
[26] L. Baillet, Y. Berthier, S. Descartes, Modelling of the Vibrations Induced by Friction. Experimental Visualisation and Identification of the Relays between the First Bodies and the Third Body, Proceedings of the European Conference on Braking, Lille, 2002, pp. 181–188.
[27] M. Godet, The third body approach : a mechanical view of wear, Wear 100 (1984) 437–452.